Acta Crystallographica Section A
Foundations of Crystallography
ISSN 0108-7673

Received 15 September 2000
Accepted 23 October 2000

Distinction between space groups having principal rotation and screw axes, which are combined with twofold rotation axes, using the coherent convergent-beam electron diffraction method

Koh Saitoh,*† Kenji Tsuda, Masami Terauchi and Michiyoshi Tanaka

Research Institute for Scientific Measurements, Tohoku University, Sendai 980-8577, Japan. Correspondence e-mail: saitohk@yamame.rism.tohoku.ac.jp

23 sets of space groups remain indistinguishable by the convergent-beam electron diffraction (CBED) method. Recently, Tsuda, Saitoh, Terauchi, Tanaka & Goodman [*Acta Cryst*. (2000), A**56**, 359–369] demonstrated that the coherent CBED method can distinguish two space-group pairs ($I23$, $I2_13$) and ($I222$, $I2_12_12_1$) by observing the relative arrangements of 2-fold-rotation and 2_1-screw axes. The other ten space-group sets, which are composed of principal rotation and screw axes and other 2-fold-rotation axes such as $P321$ and $P3_121$ ($P3_221$), are shown to be distinguishable using the coherent CBED method.

1. Introduction

Convergent-beam electron diffraction (CBED) is known as a very effective method for the determination of crystal point and space groups. Because of the strong dynamical effect of electron diffraction, it can easily find the non-centrosymmetric nature of crystals. As a result, it allows us to identify all the point groups (Goodman, 1975; Tinnappel, 1975; Buxton *et al.*, 1976; Tanaka *et al.*, 1983; Tanaka, 1989). Furthermore, CBED can distinguish between a 2-fold-rotation axis and a 2_1-screw axis, and between a mirror plane and a glide plane by observing dynamical extinction or Gjønnes–Moodie (G–M) lines (Gjønnes & Moodie, 1965; Tanaka *et al.*, 1983; Tanaka & Terauchi, 1985; Tanaka *et al.*, 1988; Tanaka, 1989). Thus, all the space groups except those listed in Table 1 can uniquely be identified (Tanaka *et al.*, 1988; Tanaka, 1989).

The space-group sets in Table 1 cannot be distinguished for the following five reasons. (i) 3_1 (3_2), 4_2 and 6_2 (6_4) screw axes cannot be distinguished from their corresponding non-screw axes because the screw axes do not form G–M lines. Thus, the space-group sets Nos. 1–5, 8, 10–13 and 18 in Table 1 cannot be distinguished. (ii) A 6_3-screw axis cannot be distinguished from a 6_1 (6_5)-screw axis because the three screw axes show G–M lines in the same manner. Thus, the space-group sets Nos. 6 and 7 cannot be distinguished. (iii) Enantiomorphic space-group pairs cannot be distinguished because they show the same CBED symmetry. Thus, the space-group pairs indicated by the parentheses in Table 1 (Nos. 1–7, 9, 19, 22 and 23) cannot be distinguished. (iv) The space-group pairs of Nos. 16 and 17 show the same CBED symmetries because they have exactly the same symmetry elements in each pair despite the different space-group symbols. (v) The space-group pairs of Nos. 14, 15, 20 and 21 cannot be distinguished because reflections that should show G–M lines due to a 4_1-screw axis are forbidden by the extinction rule of the lattice types *I* and *F*.

A practical method, however, has been used to distinguish between the rotation and screw axes, which observes intensity change of the reflections in question on tilting the specimen so that *Umweganregung* paths to the reflections disappear. This test allows us to distinguish a 3-fold-rotation axis from a 3_1 (3_2)-screw axis (Nos. 1–3), a 4-fold-rotation axis from 4_1 (4_3)- and 4_2-screw axes (Nos. 8, 10–15, 18, 20, 21) and 6-fold-rotation axis from 6_1 (6_3, 6_5)- and 6_2 (6_4)-screw axes (Nos. 4–7). The enantiomorphic space-group pairs in parentheses in Table 1, however, cannot be distinguished by this method. Identifications of the handedness of the enantiomorphic space groups were reported for quartz by Goodman & Secomb (1977) and Goodman & Johnson (1977), and for MnSi by Tanaka *et al.* (1985). Those studies were carried out by comparing the experimental intensities with the simulated ones. No qualitative method to distinguish handedness has been developed up to now.

Coherent CBED was first reported by Dowell & Goodman (1973), followed by Cowley (1979), Vine *et al.* (1992), McCallum & Rodenburg (1993), Terauchi *et al.* (1994), Tanaka *et al.* (1994), Tsuda *et al.* (1994), Steeds *et al.* (1995) and Tsuda & Tanaka (1996). A highly coherent electron beam, whose size at a focused position is smaller than a lattice spacing, illuminates a specimen with a convergence angle to overlap neighbouring reflection discs and then produces interference fringes at the overlapping regions when the beam is focused below or

† Present address: Technische Universität Darmstadt, Fachbereich Materialwissenschaft, Petersenstrasse 23, D-64287 Darmstadt, Germany.

Table 1
Space groups indistinguishable by dynamical extinction lines.

1. $P3$, $(P3_1, P3_2)$	2. $P312$, $(P3_112, P3_212)$	3. $P321$, $(P3_121, P3_221)$
4. $P6$, $(P6_2, P6_4)$	5. $P622$, $(P6_222, P6_422)$	6. $P6_3$, $(P6_1, P6_5)$
7. $P6_322$, $(P6_122, P6_522)$	8. $P4$, $P4_2$	9. $(P4_1, P4_3)$
10. $P4/m$, $P4_2/m$	11. $P4/n$, $P4_2/n$	12. $P422$, $P4_222$
13. $P42_12$, $P4_22_12$	14. $I4$, $I4_1$	15. $I422$, $I4_122$
16. $I23$, $I2_13$	17. $I222$, $I2_12_12_1$	18. $P432$, $P4_232$
19. $(P4_132, P4_332)$	20. $I432$, $I4_132$	21. $F432$, $F4_132$
22. $(P4_122, P4_322)$	23. $(P4_12_12, P4_32_12)$	

above the specimen. The positions of fringes provide phase information for crystal structure factors. Local site symmetry can be obtained from the relative positions of the interference fringe sets (Spence, 1978; Cowley, 1979; Ou & Cowley, 1988; Zuo & Spence, 1993).

Recently, Tsuda *et al.* (2000) discovered that the two special space-group pairs of ($I23$, $I2_13$) and ($I222$, $I2_12_12_1$) in the indistinguishable sets can be distinguished using the coherent CBED method by observing the difference of local site symmetries. They utilized the fact that the two space-group pairs are different with respect to the arrangements of 2-fold-rotation axes and 2_1-screw axes in the [111] projection. That is, $I23$ and $I222$ have positions at which three 2-fold-rotation axes and three 2_1-screw axes intersect, but $I2_13$ and $I2_12_12_1$ do not. Tsuda *et al.* demonstrated using computer simulations that coherent [111] CBED patterns of $I23$ and $I222$ are different from those of $I2_13$ and $I2_12_12_1$, respectively. They provided a method, for the first time, to distinguish the space-group pairs without any knowledge of the structural details.

In the case of the above sets, the principal 2-fold rotation and 2_1-screw axes are intersected perpendicularly by other

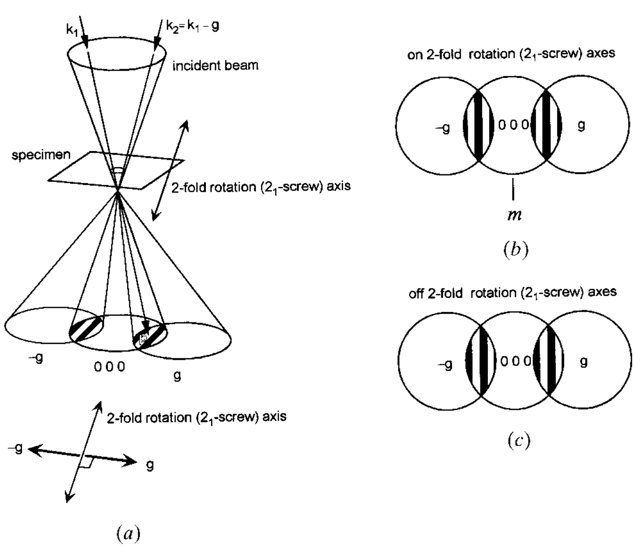

Figure 1
(*a*) Schematic drawing of the coherent CBED method for the present study. Reflection pairs $\pm\mathbf{g}$, whose diffraction vectors are perpendicular to the direction of the 2-fold-rotation (2_1-screw) axis are used. Interference fringes are formed in the overlapping regions of adjacent reflection discs. Mirror symmetry is seen (*b*) when the probe is located on a 2-fold-rotation (2_1-screw) axis, but is not seen (*c*) when the probe is not on the 2-fold-rotation (2_1-screw) axis.

2-fold rotation axes and 2_1-screw axes (hereafter referred to as 2 axes and 2_1 axes). Tsuda *et al.*'s analysis has the potential to be extensively applied to the distinction of space groups that have principal 3-, 4- and 6-fold rotation and screw axes accompanied by perpendicular 2-fold rotation axes such as $P321$ and $P3_121$ ($P3_221$), or to the ten space-group sets of Nos. 2, 3, 5, 7, 12, 13, 15, 18, 20, 21 in Table 1. In the present paper, we clarify theoretically that the ten space-group sets can be distinguished by the coherent CBED method.

2. Identification of the intersecting positions of 2-fold-rotation axes by coherent CBED

Fig. 1(*a*) shows a schematic diagram of the coherent CBED method. A convergence angle of the incident beam is set to overlap the neighbouring reflection discs. Two plane waves with wave vectors of $\mathbf{k}_1$ and $\mathbf{k}_2 = \mathbf{k}_1 - \mathbf{g}$ form interference fringes at $\mathbf{p}$ in the overlapping region. If the focused point of the incident beam is on the specimen, each overlapping region of the CBED discs shows a uniform intensity. If the beam is defocused from the specimen, interference fringes appear in the overlapping regions. Formation of the interference fringes was explained in detail by Cowley (1979), Vine *et al.* (1992) and Terauchi *et al.* (1994). The entire fringe set displaces with a shift of the probe position. The relative position of the fringes is determined by the probe position and the phase difference between the crystal structure factors of the reflections. The former effect is described by a phase factor of $\exp(2\pi i\mathbf{g}\cdot\Delta\mathbf{r})$, where $\mathbf{g}$ and $\Delta\mathbf{r}$ respectively indicate a reflection vector and a vector pointing to the probe position from the origin of a unit cell.

For the present study, we consider the interference fringes between the transmitted wave (000) and its two neighbouring reflected waves ($\pm\mathbf{g}$), whose diffraction vectors are perpendicular to the direction of the 2 axis (Fig. 1*a*). It is noted that the 2 axes are not necessarily perpendicular to the incident-beam direction (Tsuda *et al.*, 2000). When the probe is located on the 2 axis, the phase of the crystal structure factors and that for the probe position are the same for the two reflections. As a result, the two interference-fringe sets appearing in the two overlapping regions show mirror symmetry *m* with respect to the transmitted beam as shown in Fig. 1(*b*). If the probe is not on the axis, the fringe sets do not show mirror symmetry as shown in Fig. 1(*c*). Thus, we can identify the position of the 2 axis from the coherent CBED pattern. The positions of the 2 axes in the other orientations are examined using the reflection pairs whose diffraction vectors are perpendicular to the 2 axes. If the probe is put on an intersection point of two 2 axes, the coherent CBED pattern shows two sets of mirror symmetry. Similarly, the coherent CBED pattern shows three sets of mirror symmetry at an intersection point of three 2 axes. Therefore, the intersection points of the 2 axes can be revealed by observing the interference fringes in the coherent CBED patterns. It is noted that two fringe sets in a reflection pair are shifted in the same manner by a shift of the probe position.

3. Distinction of space groups

3.1. Space groups $P321$ and $P3_121$ ($P3_221$) [$P312$ and $P3_112$ ($P3_212$)]

Distinction of space-group set No. 3 is investigated here as an example. Space-group set No. 2 can also be distinguished by the same procedure. Figs. 2(*a*), 2(*b*) and 2(*c*) schematically show the arrangements of 2 axes of space groups $P321$, $P3_121$ and $P3_221$ projected along the [0001] direction. The thin lines indicate 2 axes and thick lines the unit cell. The fractional numbers beside the thin lines indicate fractional coordinates of the 2 axes in the [0001] direction. There are three 2 axes perpendicular to the [0001] direction, two of which form an angle of 120° degrees. The three 2 axes are at the same height in the [0001] direction for $P321$. They, however, are separated by $c/6$ in the [0001] direction with a 120° clockwise rotation for $P3_121$ and with a counter-clockwise rotation for $P3_221$. Since the three space groups have the same arrangement of the three 2 axes when they are projected in the [0001] direction, the space groups cannot be distinguished in this projection.

Table 2 shows atomic coordinates of the general positions, relations between the structure factors and kinematical extinction rules for the space groups $P321$, $P3_121$ and $P3_221$ (*International Tables for X-ray Crystallography*, 1952). The

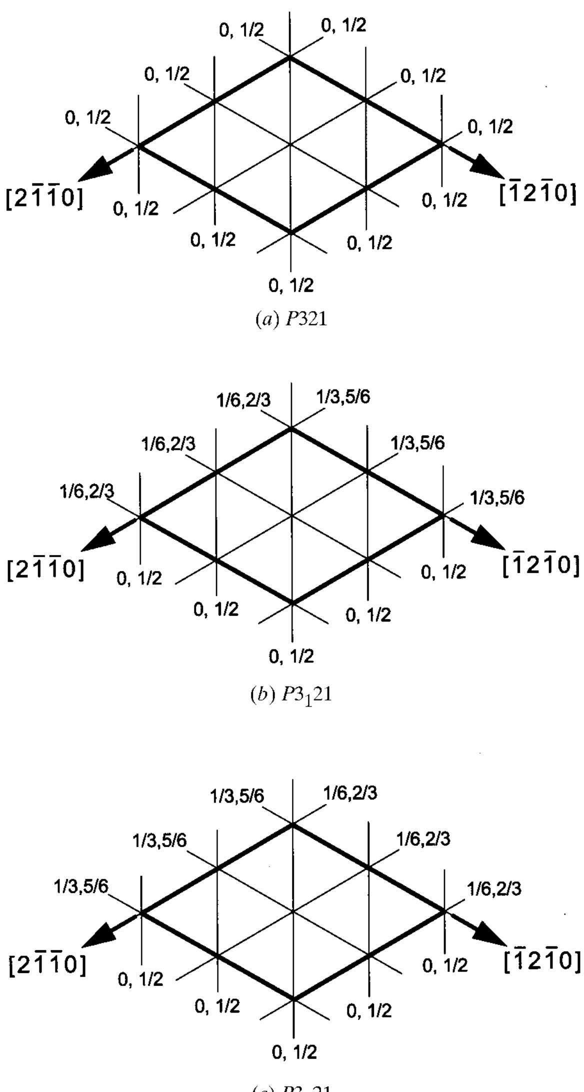

Figure 2
Arrangements of 2-fold rotation axes of (*a*) $P321$, (*b*) $P3_121$ and (*c*) $P3_221$ projected along the [0001] zone axis.

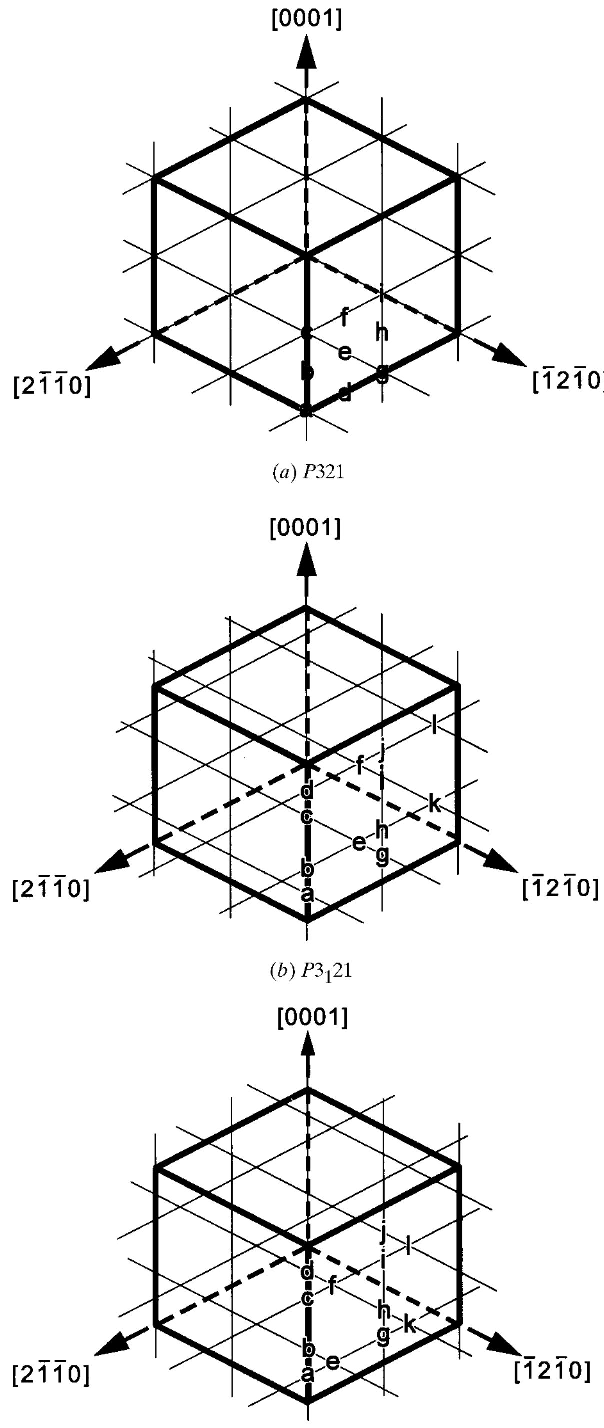

Figure 3
Arrangements of 2-fold-rotation axes of (*a*) $P321$, (*b*) $P3_121$ and (*c*) $P3_221$ projected along the $[11\bar{2}3]$ zone axis.

Table 2
Atom coordinates of the general positions, relations between the structure factors and kinematical extinction rules for the space groups (*a*) $P321$, (*b*) $P3_121$ and (*c*) $P3_221$.

(*a*) $P321$
Atom coordinates:
$|x, y, z; \bar{y}, x-y, z; y-x, \bar{x}, z; y, x, \bar{z}; \bar{x}, y-x, \bar{z}; x-y, \bar{y}, \bar{z}|$
Relations between structure factors:
$|F(hkl)| = |F(\bar{h}\bar{k}\bar{l})| = |F(kil)| \neq |F(\bar{h}kl)| \neq |F(h\bar{k}l)| \neq |F(hk\bar{l})| = |F(khl)|$
$\alpha(hkl) = \alpha(\bar{h}\bar{k}\bar{l}) = \alpha(kil) \neq \alpha(\bar{h}kl) \neq \alpha(h\bar{k}l) \neq \alpha(hk\bar{l}) = \alpha(khl)$
Kinematical extinction rule:
No conditions

(*b*) $P3_121$
Atom coordinates:
$|x, y, z; \bar{y}, x-y, 1/3+z; y-x, \bar{x}, 2/3+z; y, x, \bar{z}; \bar{x}, y-x, 1/3-z; x-y, \bar{y}, 2/3-z|$
Relations between structure factors:
$|F(hkl)|$ relationships as for $P321$
$\alpha(hkl) = -\alpha(\bar{h}\bar{k}\bar{l}) \neq \alpha(\bar{h}kl) \neq \alpha(h\bar{k}l) \neq \alpha(hk\bar{l}) = \alpha(khl)$
$l = 3n$ $\qquad$ $\alpha(hkl) = \alpha(kil)$
$l = 3n \pm 1$ $\qquad$ $\alpha(hkl) = \alpha(kil) \pm 2/3\pi$
Kinematical extinction rule:
$l = 3n \pm 1$ and $h = k = 0$

(*c*) $P3_221$
Atom coordinates:
$|x, y, z; \bar{y}, x-y, 2/3+z; y-x, \bar{x}, 1/3+z; y, x, \bar{z}; \bar{x}, y-x, 2/3-z; x-y, \bar{y}, 1/3-z|$
Relations between structure factors:
$|F(hkl)|$ relationships as for $P321$
$\alpha(hkl) = -\alpha(\bar{h}\bar{k}\bar{l}) \neq \alpha(\bar{h}kl) \neq \alpha(h\bar{k}l) \neq \alpha(hk\bar{l}) = \alpha(khl)$
$l = 3n$ $\qquad$ $\alpha(hkl) = \alpha(kil)$
$l = 3n \pm 1$ $\qquad$ $\alpha(hkl) = \alpha(kil) \mp 2/3\pi$
Kinematical extinction rule:
$l = 3n \pm 1$ and $h = k = 0$

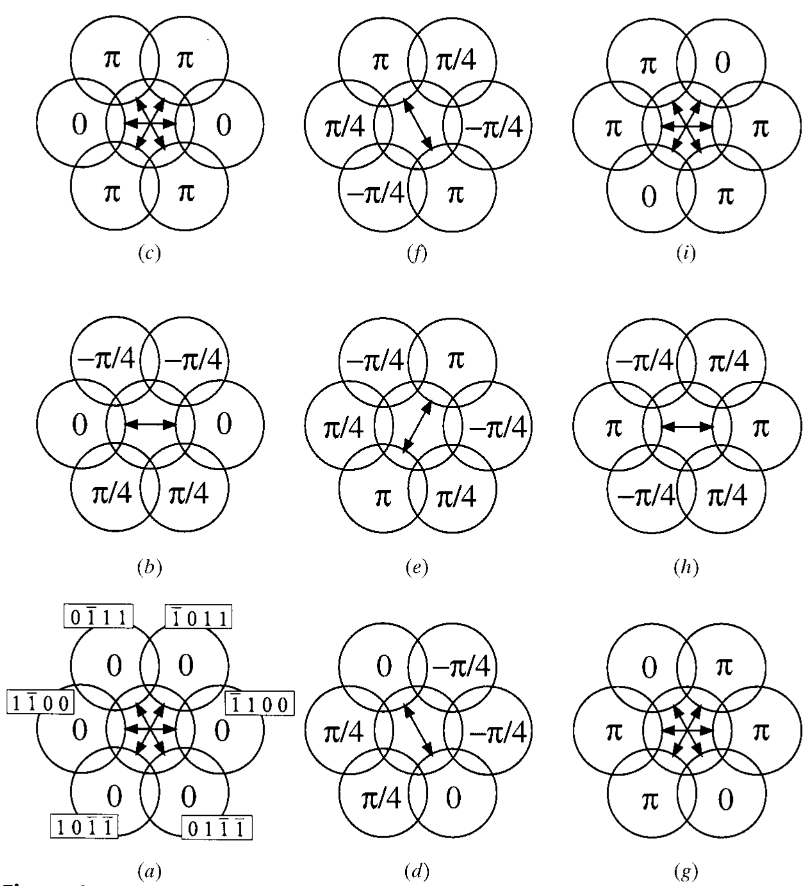

Figure 4
Phases of the kinematical crystal structure factors of the $P321$ model of Table 3 for the electron probe positions *a*–*i* illustrated in Fig. 3(*a*).

relations between the phases of the structure factors are different for the three space groups.

Figs. 3(*a*), 3(*b*) and 3(*c*), respectively, show the arrangements of the 2 axes of space groups $P321$, $P3_121$ and $P3_221$ projected along the $[11\bar{2}3]$ direction. It can be seen in this projection that the arrangements of the three 2 axes are different for the three space groups. $P321$ has points where the three 2 axes intersect (*a*, *c*, *g* and *i*). $P3_121$ and $P3_221$ do not have such points but have points where only two of the three 2 axes intersect (*a*–*l*). Conventional CBED patterns taken at $[11\bar{2}3]$ incidence do not show any symmetry because these 2 axes are neither parallel nor perpendicular to the incident beam but coherent CBED shows different symmetries for $P321$, $P3_121$ and $P3_221$, allowing us to distinguish them.

Table 3 shows the model structures of space groups $P321$, $P3_121$ and $P3_221$, which are used for the simulations of coherent CBED patterns. These models are produced by placing Si and C atoms respectively at general positions (0.18,0.20,0.15) and (0.25,0.10,0.05) and by generating atoms using the symmetry operations of the space groups. Fig. 4 schematically shows the resultant phases of crystal structure factors and probe positions for the six diffracted waves at probe positions *a*–*i* denoted in Fig. 3(*a*) for the model of $P321$. Figs. 5 and 6 similarly show those phases at the probe positions *a*–*l* in Figs. 3(*b*) and 3(*c*) for the models of $P3_121$ and $P3_221$, respectively. It is seen that the phases of the reflections $\pm\mathbf{g}$ perpendicular to a 2 axis are the same as indicated by the arrows when the probe is located on the 2 axis.

Figs. 7(*a*)–7(*i*) show coherent CBED simulation patterns of the model of $P321$ under a kinematical approximation for the electron probe positions at *a*–*i* in Fig. 3(*a*), respectively. At positions *a*, *c*, *g* and *i*, there appear three sets of mirror symmetry, clarifying these positions to be the intersection points of the three 2 axes. Figs. 8(*a*)–8(*l*) show coherent CBED patterns of the model of $P3_121$ at positions *a*–*l* in Fig. 3(*b*). Two of the three fringe pairs show mirror symmetry but no three fringe pairs show mirror symmetry. Figs. 9(*a*)–9(*l*) show coherent CBED patterns of the model of $P3_221$ for positions *a*–*l* in Fig. 3(*c*). Only two of the three fringe pairs show mirror symmetry as well as those of $P3_121$, clarifying that the two 2 axes intersect at those positions. Therefore, $P321$ can be distinguished from $P3_121$ and $P3_221$ by the examination of the mirror symmetry sets using the coherent CBED method. It is clear that space-group set No. 2 can be distinguished in the same manner at the $[10\bar{1}1]$ electron incidence because the 2 axes of $P312$,

Table 3
Model structures of $P321$, $P3_121$ and $P3_221$ used for simulations of coherent CBED patterns.

Space group	Site	Element	(x, y, z)	Lattice parameter (nm)
$P321$	$6(g)$	Si	(0.18, 0.20, 0.15)	$a = 0.4$, $c = 0.8$
	$6(g)$	C	(0.25, 0.10, 0.05)	
$P3_121$	$6(c)$	Si	(0.18, 0.20, 0.15)	$a = 0.4$, $c = 0.8$
	$6(c)$	C	(0.25, 0.10, 0.05)	
$P3_221$	$6(c)$	Si	(0.18, 0.20, 0.15)	$a = 0.4$, $c = 0.8$
	$6(c)$	C	(0.25, 0.10, 0.05)	

Table 4
Model structures of $P622$, $P6_222$ and $P6_422$ used for simulations of coherent CBED patterns.

Space group	Site	Element	(x, y, z)	Lattice parameter (nm)
$P622$	$12(n)$	Si	(0.18, 0.20, 0.15)	$a = 0.4$, $c = 0.8$
	$12(n)$	C	(0.25, 0.10, 0.05)	
$P6_222$	$12(k)$	Si	(0.20, 0.21, 0.15)	$a = 0.4$, $c = 0.8$
	$12(k)$	C	(0.31, 0.10, 0.05)	
$P6_422$	$12(k)$	Si	(0.20, 0.21, 0.15)	$a = 0.4$, $c = 0.8$
	$12(k)$	C	(0.31, 0.20, 0.05)	

$P3_112$ and $P3_212$ are located at orientations different by 30° from those of $P321$, $P3_121$ and $P3_221$.

3.2. The other space groups (Nos. 5, 7, 12, 13, 15, 18, 20 and 21)

Similar examinations prove that the space groups of the other sets of Nos. 5, 7, 12, 13, 15, 18, 20 and 21 in Table 1 can be distinguished.

3.2.1. $P622$ and $P6_222$ ($P6_422$) [$P6_322$ and $P6_122$ ($P6_522$)]. For the space-group sets of the hexagonal lattice system (Nos. 5 and 7), the $[11\bar{2}3]$ electron incidence is suitable for their distinction. Distinction of space-group set No. 5 is described as an example. Space group set No. 7 is distinguished by the same procedure. Figs. 10(a), 10(b) and 10(c) show all of the six 2 (2_1)-axis arrangements of space groups $P622$, $P6_222$ and $P6_422$ in the $[11\bar{2}3]$ projection. Figs. 10(d), 10(e) and 10(f) show the arrangements of the three observable 2 (2_1) axes, when three reflection pairs ($1\bar{1}00$, $\bar{1}100$), ($0\bar{1}11$, $01\bar{1}\bar{1}$) and ($10\bar{1}\bar{1}$, $\bar{1}011$), which are the first- and second-nearest-neighbour reflections to the transmitted beam, are used for observing the interference fringes. The arrangements are completely the same as those of $P321$, $P3_221$ and $P3_121$ (Figs. 2a, 2c and 2b), that is, $P622$ has points where the three observable 2 (2_1) axes intersect (a, c, i and k), whereas $P6_222$ and $P6_422$ do not have such points but have points at which only the two 2 (2_1) axes intersect (a, b and d). Thus, $P622$, $P6_222$ and $P6_422$ can be distinguished by the coherent CBED method by the same procedure as $P321$, $P3_121$ and $P3_221$ can be. Table 4 shows the model structures of space groups of $P622$, $P6_222$ and $P6_422$ for simulations. Figs. 11(a), 11(b) and 11(c) show the simulation patterns from the models of $P622$, $P6_222$ and $P6_422$ at position a of each unit cell. The coherent CBED pattern of $P622$ shows three sets of mirror symmetry, whereas those of $P6_222$ and $P6_422$ show only two sets of mirror symmetry, as indicated by the arrows. It should be noted that the appearances of mirror symmetry are the same as those of $P321$ (Fig. 7a), $P3_221$ (Fig. 9a) and $P3_121$ (Fig. 8b). We examined the fact that simulation patterns of $P622$, $P6_222$ and $P6_422$ at other probe positions show the same symmetry sets as $P321$, $P3_121$ and $P3_221$. Thus, space group $P622$ can be distinguished from $P6_222$ and $P6_422$ by the coherent CBED method. $P6_322$, $P6_122$ and $P6_522$ have the same 2 (2_1)-axis arrangements as those of $P622$, $P6_422$ and $P6_222$ in the $[11\bar{2}3]$ projection, as far as the 2 (2_1) axes concerned with the first- and second-nearest-neighbour reflections are considered. Thus, $P6_322$ can also be distinguished from $P6_122$ and $P6_522$ by the same procedure.

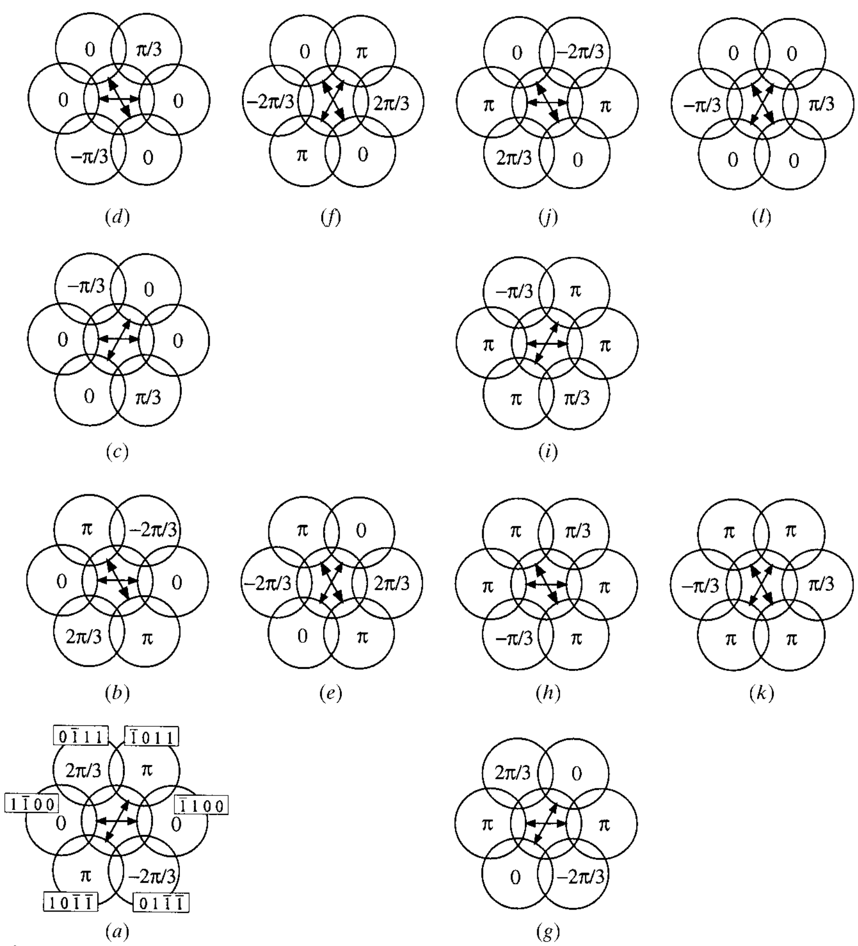

Figure 5
Phases of the kinematical crystal structure factors of the $P3_121$ model of Table 3 for the electron probe positions a–l illustrated in Fig. 3(b).

Table 5
Model structures of $P422$ and $P4_222$ used for simulations of coherent CBED patterns.

Space group	Site	Element	(x, y, z)	Lattice parameter (nm)
$P422$	$8(p)$	Si	(0.23, 0.30, 0.15)	$a = 0.4$, $c = 0.8$
	$8(p)$	C	(0.08, 0.12, 0.05)	
$P4_222$	$8(p)$	Si	(0.18, 0.25, 0.15)	$a = 0.4$, $c = 0.8$
	$8(p)$	C	(0.07, 0.15, 0.05)	

3.2.2. $P422$ and $P4_222$ ($P42_12$ and $P4_22_12$). For the space-group set of No. 12 ($P422$, $P4_222$), the [211] incidence is suitable for the distinction. Figs. 12(*a*) and 12(*b*) show the arrangements of the three observable 2 (2_1) axes when three reflection pairs ($0\bar{1}1, 01\bar{1}$), ($10\bar{2}, \bar{1}02$) and ($1\bar{1}\bar{1}, \bar{1}11$), which are respectively the first-, second- and third-nearest-neighbour reflections to the transmitted beam, are used for observing the coherent fringes. It is seen that $P422$ has points where the three 2 (2_1) axes intersect, whereas $P4_222$ does not have such points but has points where only the two 2 (2_1) axes intersect. It should be noted that the 2 (2_1)-axis arrangements are similar to those of $I23$ ($I222$) and $I2_13$ ($I2_12_12_1$) in the [111] projection as shown in Figs. 3(*a*) (Fig. 9*a*) and 3(*b*) (Fig. 9*b*) of the paper by Tsuda *et al.* (2000). Figs. 13(*a*) and 13(*b*) show coherent CBED patterns simulated at the origins O of the unit cells for the models of $P422$ and $P4_222$, whose atomic arrangements are generated from the atom positions listed in Table 5 by the symmetry operations of the space groups. The coherent CBED pattern of $P422$ shows three sets of mirror symmetry but that of $P4_222$ shows only two of them as indicated by the arrows. It should be pointed out that the simulation patterns show the same features of mirror symmetry as those of $I23$ ($I222$) and $I2_13$ ($I2_12_12_1$) simulated at the origins of the unit cells [Figs. 6(*a*) and 12(*a*) of Tsuda *et al.* (2000), respectively]. We examined that simulation patterns of $P422$ and $P4_222$ at other positions show the same symmetry as those of $I23$ ($I222$) and $I2_13$ ($I2_12_12_1$). Thus, $P422$ can be distinguished from $P4_222$ by the coherent CBED method.

For the distinction of the space-group set of No. 13 ($P42_12$ and $P4_22_12$), similarly the [211] incidence is available. The relative 2 (2_1)-axis arrangements of $P42_12$ and $P4_22_12$, which are observable with three reflection pairs ($0\bar{1}1, 01\bar{1}$), ($10\bar{2}, \bar{1}02$) and ($1\bar{1}\bar{1}, \bar{1}11$) are the same as those of $P422$ and $P4_222$, respectively. Thus, space group $P42_12$ can be distinguished from $P4_22_12$ by the same procedure as that for the space groups $P422$ and $P4_222$.

3.2.3. $I422$ and $I4_122$ ($I432$ and $I4_132$). For the space-group set of No. 15 ($I422$, $I4_122$), the [111] electron incidence is available for the distinction. In the [111] projection, the 2 (2_1)-axis arrangements of $I422$ and $I4_122$, which are observable using three reflection pairs ($0\bar{1}1, 01\bar{1}$), ($10\bar{1}, \bar{1}01$) and ($\bar{1}10, 1\bar{1}0$) neighbouring to the transmitted beam, are similar to those of $P422$ and $P4_122$, respectively (see Figs. 16*a* and 16*b*). That is, $I422$ has points where the three 2 (2_1) axes intersect (*a*–*d* in Fig. 16*a*), but $I4_122$ does not. It was examined that simulation patterns of $I422$ and $I4_122$ show the same sets of mirror symmetry as those of $P422$ and $P4_222$. Thus, they are

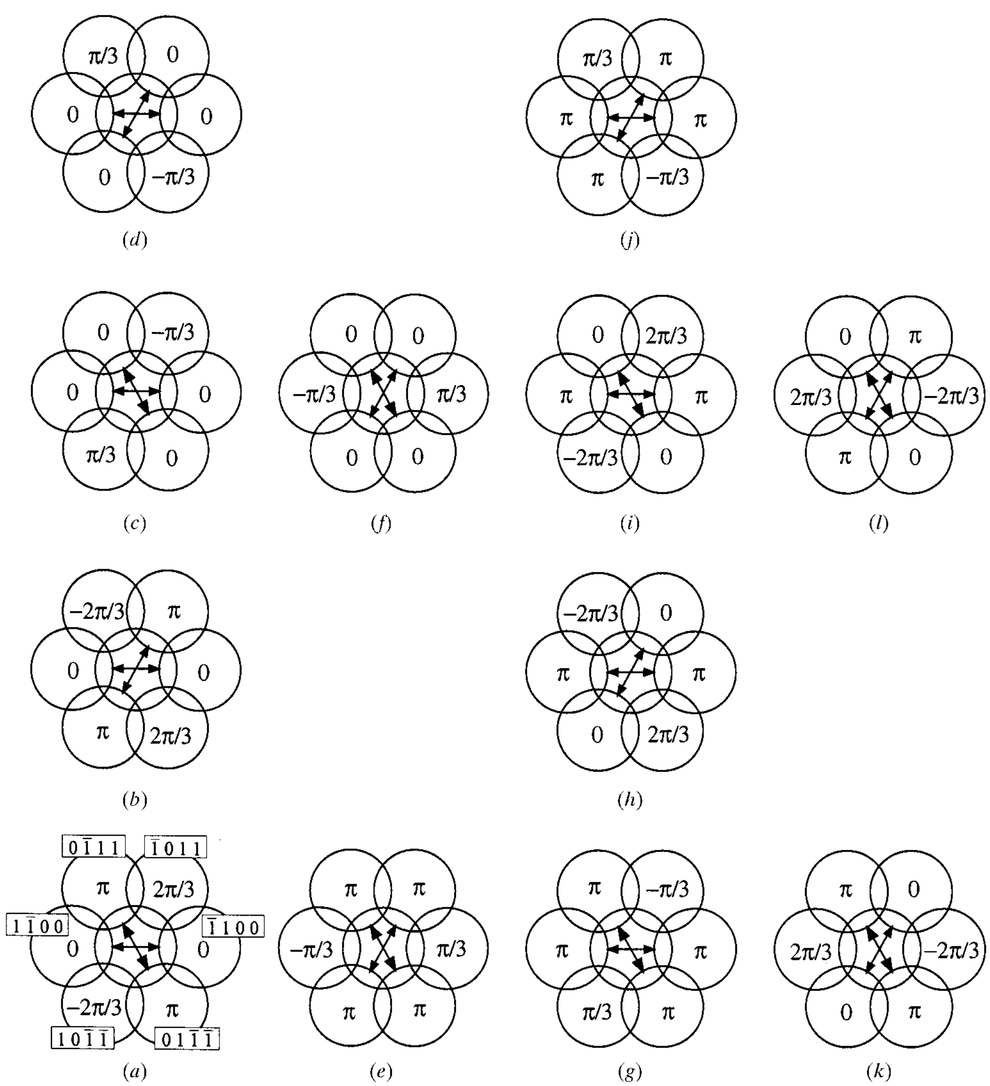

Figure 6
Phases of the kinematical crystal structure factors of the $P3_221$ model of Table 3 for the electron probe positions *a*–*l* illustrated in Fig. 3(*c*).

distinguished in the same procedure as the distinction between $P422$ and $P4_222$.

For the distinction of the space-group set of No. 20 ($I432$, $I4_132$), similarly the [111] electron incidence is available. 2 (2_1)-axis arrangements of space groups $I432$ and $I4_132$, which are observable using three reflection pairs ($0\bar{1}1, 01\bar{1}$), ($10\bar{1}, \bar{1}01$) and ($\bar{1}10, 1\bar{1}0$), are similar to those of $I422$ and $I4_122$, respectively. It was examined that simulation patterns of $I432$ and $I4_132$ show the same sets of mirror symmetry as those of $I422$ and $I4_222$. Thus, $I432$ is distinguished from $I4_132$ by the same procedure as that of $I422$ and $I4_222$.

3.2.4. *P*432 and *P*4$_2$32. For the space-group set of No. 18 ($P432$, $P4_232$), the [321] electron incidence is available for the distinction. In the [321] projection, the 2 (2_1)-axis arrangements of $P432$ and $P4_232$ observable using three reflection pairs ($1\bar{1}\bar{1}, \bar{1}11$), ($0\bar{1}2, 01\bar{2}$) and ($1\bar{2}1, \bar{1}2\bar{1}$), which are neighbouring reflections to the transmitted beam, are similar to those of $P422$ and $P4_222$, respectively. It was confirmed that simulation patterns of $P432$ show three sets of mirror symmetry but those of $P4_232$ show only two of them. Thus, $P432$ can be distinguished from $P4_232$ in the same procedure as the distinction between $P422$ and $P4_222$.

3.2.5. *F*432 and *F*4$_1$32. For the space-group set of No. 21 ($F432$, $F4_132$), the [432] electron incidence is available to distinguish them. The 2 (2_1)-axis arrangements of $F432$ and $F4_132$ in this projection, which are observable using the first-, second- and third-nearest-neighbour reflection pairs to the transmitted beam, or ($\bar{2}04, 20\bar{4}$), ($\bar{2}4\bar{2}, 2\bar{4}2$) and ($\bar{4}42, 4\bar{4}\bar{2}$) are

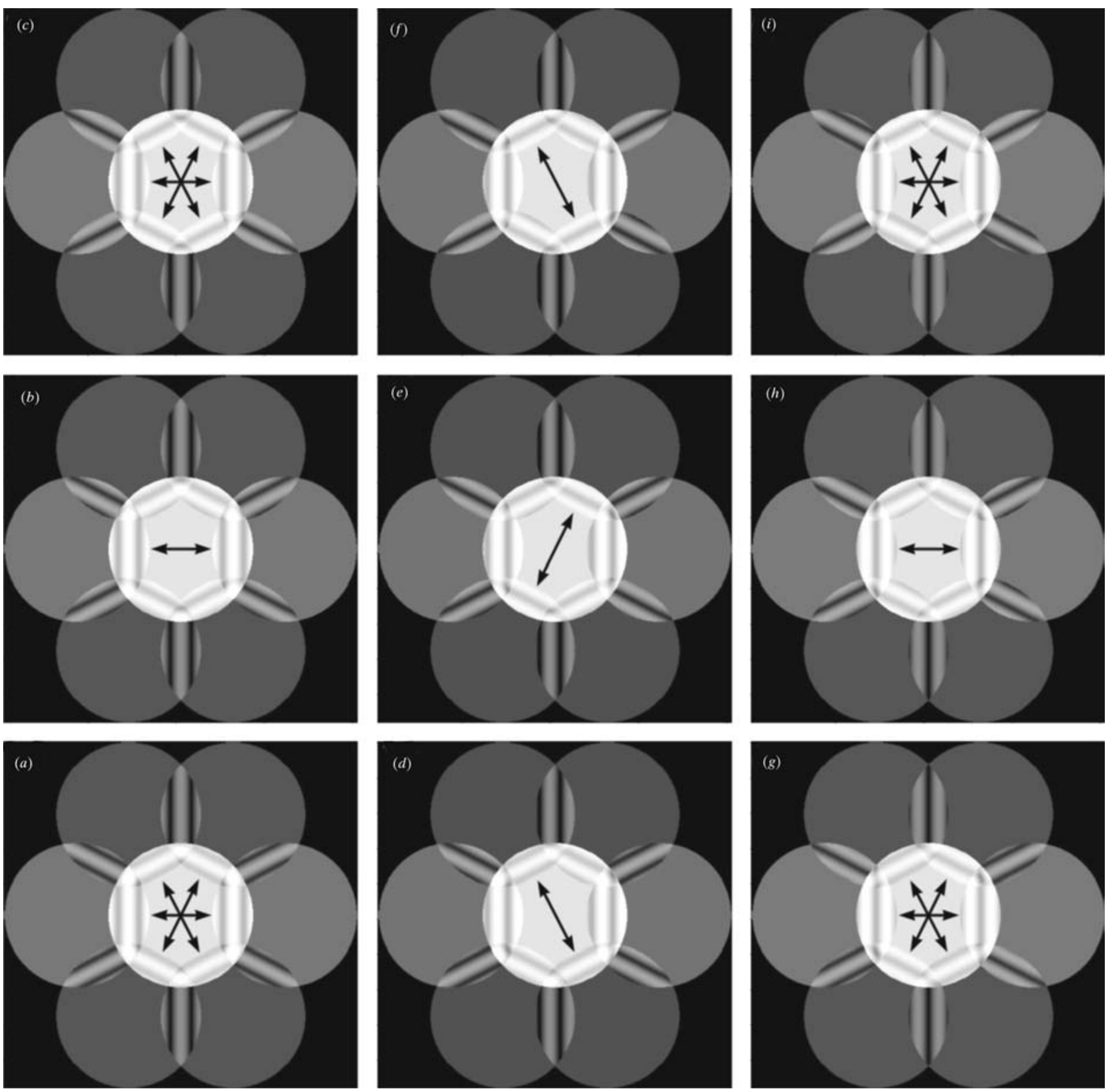

Figure 7
[$11\bar{2}3$] coherent CBED patterns simulated for the $P321$ model for the electron probe positions *a*–*i* of Fig. 3(*a*). The pairs of overlapping areas with the same contrast are indicated by pairs of arrows. (*a*), (*c*), (*g*) and (*i*) exhibit three sets of such pairs, conforming the intersection of three 2 (2_1) axes at positions *a*, *c*, *g* and *i* in Fig. 3(*a*).

similar to those of the observable 2 (2_1) axes of $P422$ and $P4_222$, respectively. We confirmed that simulation patterns of $F432$ show three sets of mirror symmetry but those of $F4_222$ show only two sets. Thus, $F432$ can be distinguished from $F4_132$ in the same procedure as the distinction between $P422$ and $P4_222$.

4. Discussion

The electron incidences chosen in the previous section allow us to distinguish the space groups using interference fringes formed by the transmitted beam and one of its neighbouring diffracted beams. Unfortunately, some of those incidences have relatively high order indices such as [432], which may not be preferable from the experimental viewpoint. Low-order incidences can also be available for the distinction if we observe interference fringes formed by the transmitted beam and diffracted beams, which are not neighbouring to the transmitted beam. For example, the [112] incidence is useful for the distinction between $P422$ and $P4_222$. In this projection, $P422$ has points where four 2 (2_1) axes intersect (*a* and *b*) but $P4_222$ does not, as shown in Figs. 14(*a*) and 14(*b*), respectively. Thus, coherent CBED patterns composed of four reflection pairs $(1\bar{1}0, \bar{1}10)$, $(11\bar{1}, \bar{1}\bar{1}1)$, $(01\bar{2}, 20\bar{1})$ and $(0\bar{2}1, 02\bar{1})$ can reveal the difference of the 2 (2_1)-axis arrangements through the different sets of mirror symmetry. The reflection pairs of $(1\bar{1}0, \bar{1}10)$, $(11\bar{1}, \bar{1}\bar{1}1)$, $(\bar{2}01, 20\bar{1})$ and $(0\bar{2}1, 02\bar{1})$ are the first-, second- and third-nearest-neighbour ones in the present

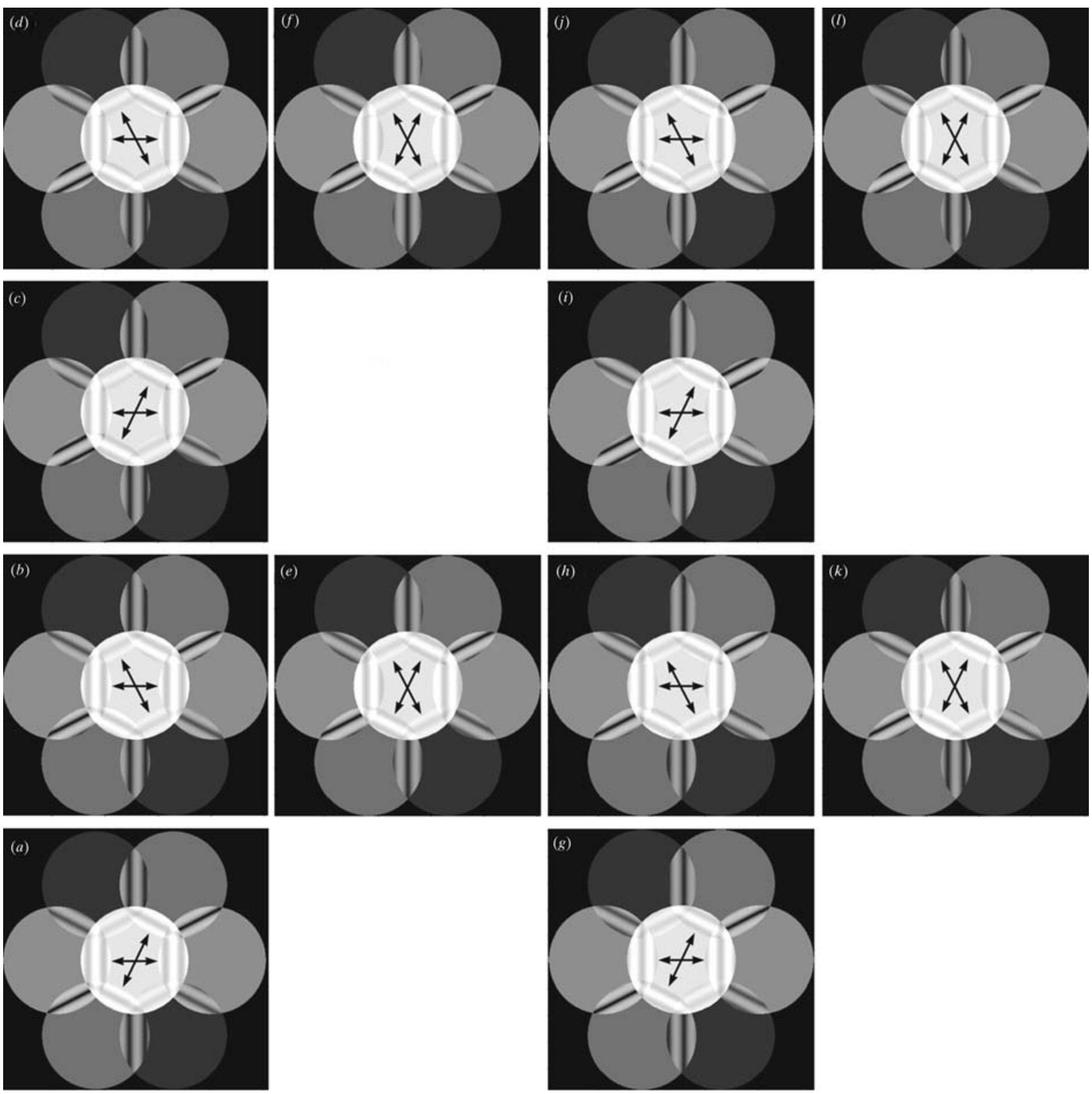

Figure 8
$[11\bar{2}3]$ coherent CBED patterns simulated for the $P3_121$ model for the electron probe positions *a*–*l* of Fig. 3(*b*). The pairs of overlapping areas with the same contrast are indicated by pairs of arrows. Only two sets of such pairs are seen in (*a*)–(*l*), indicating the absence of intersection of three 2 (2_1) axes.

model, whose reflection vectors are perpendicular to the 2 (2_1) axes. Figs. 15(*a*) and 15(*b*) show coherent CBED patterns simulated at the [112] incidence for models of *P*422 and $P4_222$ with probe positions *a* denoted in Figs. 14(*a*) and 14(*b*) (the origins of the unit cells). The simulation pattern of *P*422 shows four sets of mirror symmetry, but that of $P4_222$ shows only three sets of them, as indicated by the arrows. Thus, the [112] incidence can also be available for their distinction. It should be noted in this case that the 201-type reflections are overlapped not only with the transmitted disc but also with the 110- and 111-type reflection discs. Thus, the fringe patterns in the overlapping regions are formed by the interferences of these beams. At an intersecting point of two 2 (2_1) axes, phases of the reflection pair perpendicular to each 2 (2_1) axis are the same. Thus, the interference fringes in the overlapping regions of these reflection discs show mirror symmetry at the intersecting point because the positions of the fringes can simply be determined by the sum of the phases of the overlapping reflections. Therefore, the 2 (2_1)-axis arrangements can be observed by mirror symmetry of many-beam interference fringes as well as those of two-beam interference fringes. The electron incidences available for the distinction of the space-group sets described above are summarized in Table 6. The indices with an asterisk indicate the incidences at which the distinction is performed by many-beam interference.

In the distinction procedures described above, the electron probe has to be located at the points where a plural number of 2 (2_1) axes intersect. We found a method to distinguish the

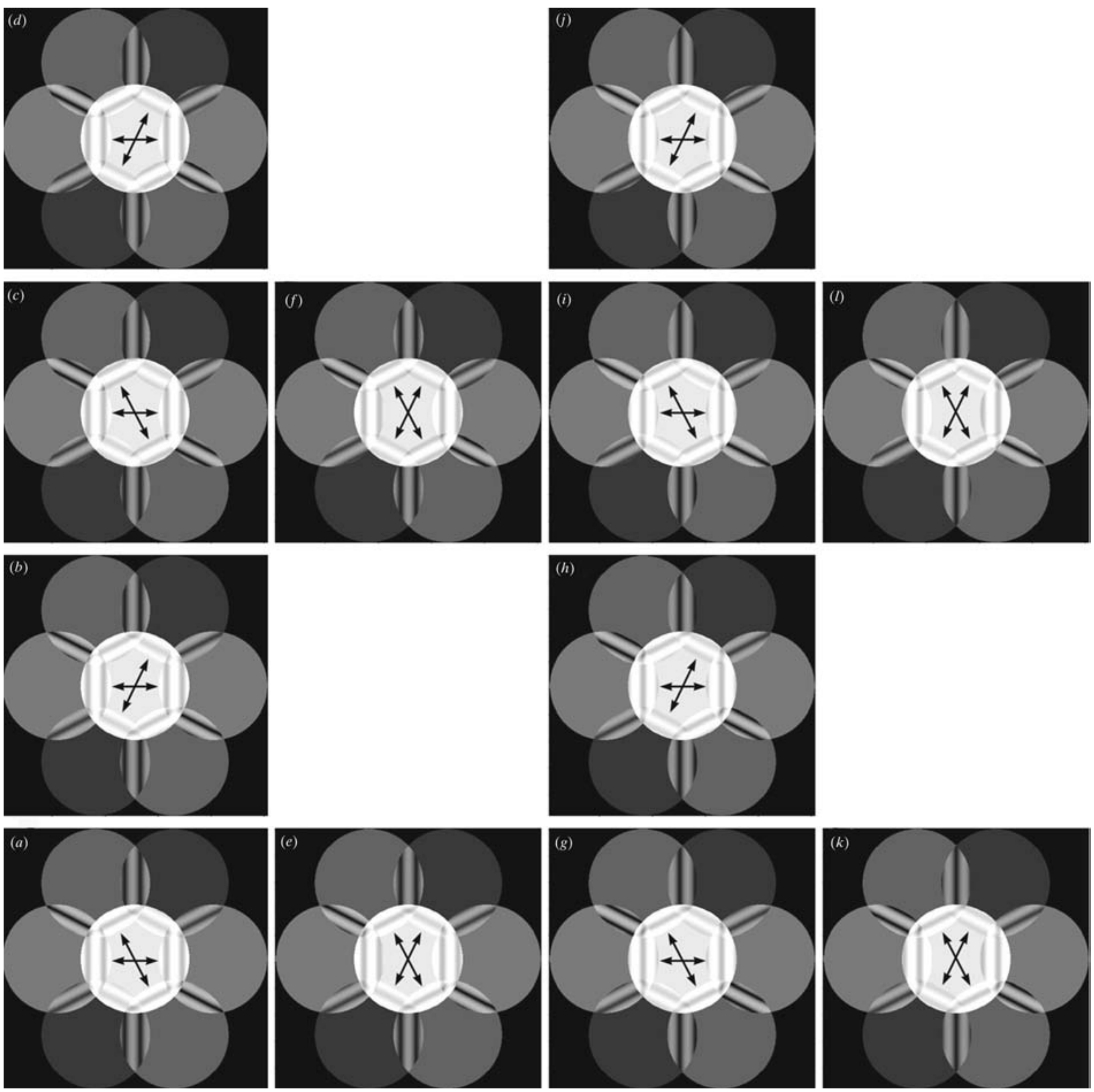

Figure 9
[11$\bar{2}$3] coherent CBED patterns simulated for the $P3_221$ model for the electron probe positions *a*–*l* of Fig. 3(*c*). Only two sets of such pairs are seen in (*a*)–(*l*), indicating the absence of intersection of three 2 (2_1) axes as in Fig. 8.

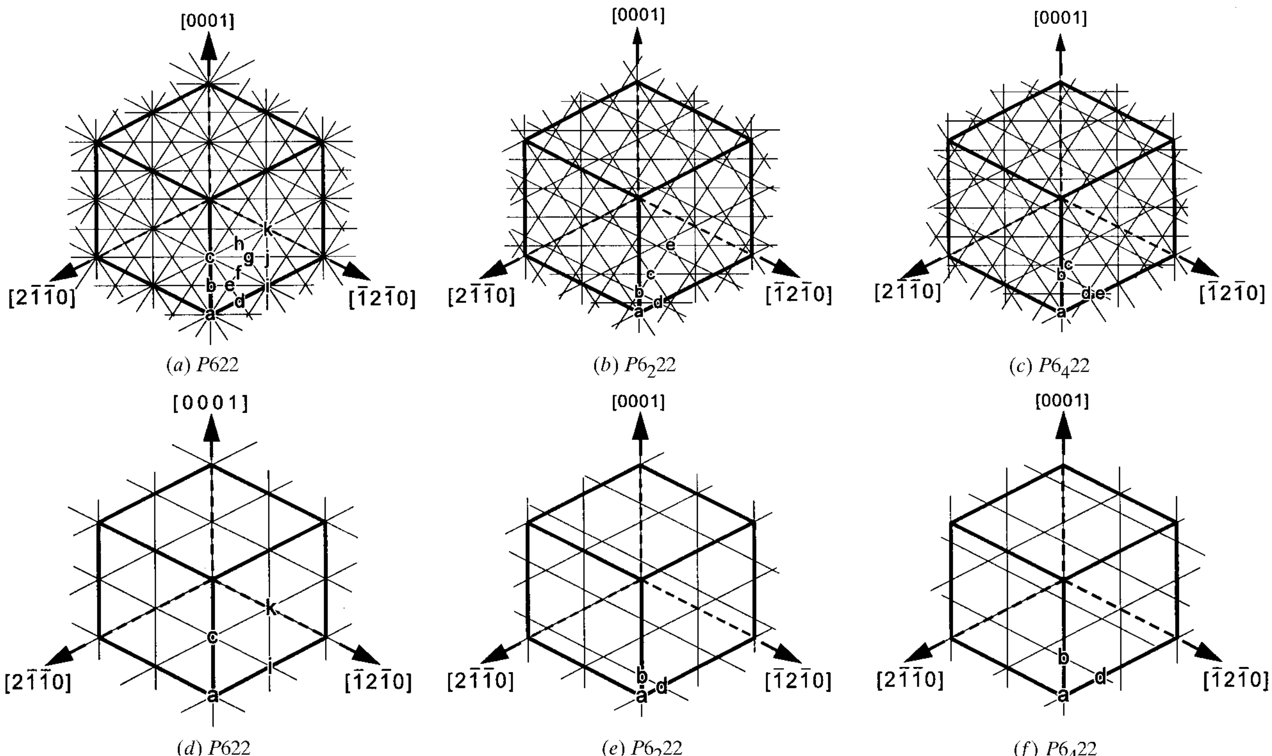

Figure 10
Arrangements of 2-fold-rotation and 2_1-screw axes of (*a*) *P*622, (*b*) $P6_222$ and (*c*) $P6_422$ projected along the [11$\bar{2}$3] zone axis. Arrangements of observable 2-fold-rotation and 2_1-screw axes using three reflection pairs $(1\bar{1}00, \bar{1}100)$, $(01\bar{1}1, 01\bar{1}\bar{1})$ and $(10\bar{1}1, \bar{1}011)$ of (*d*) *P*622, (*e*) $P6_222$ and (*f*) $P6_422$.

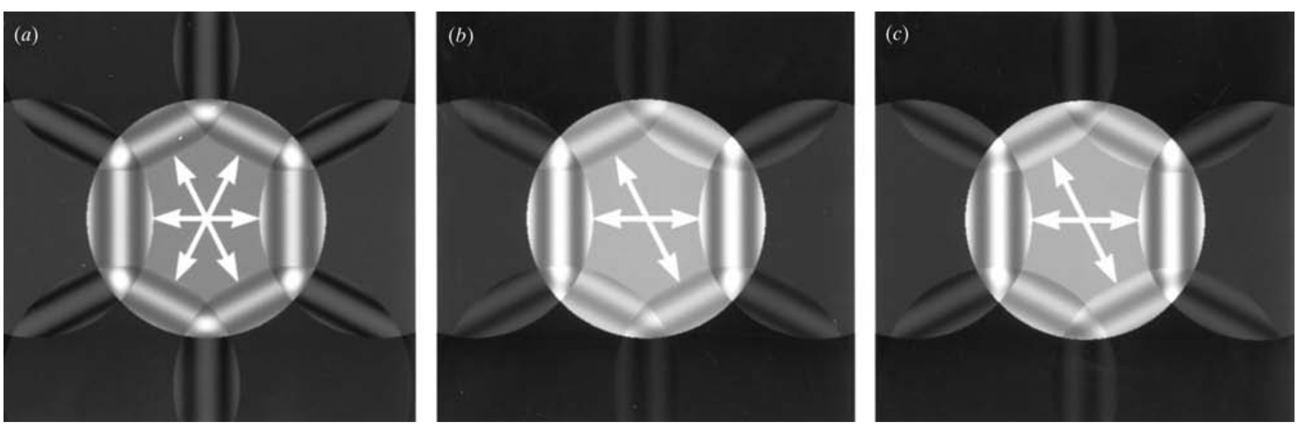

Figure 11
[11$\bar{2}$3] coherent CBED patterns simulated for the *P*622, $P6_222$ and $P6_422$ models for the electron probe positions *a* of Figs. 10(*a*), 10(*b*) and 10(*c*). The pairs of overlapping areas with the same contrast are indicated by pairs of arrows. (*a*) exhibits three sets of such pairs, conforming to the intersection of three 2 (2_1) axes at position *a* in Fig. 10(*a*), but (*b*) and (*c*) show only two sets of such pairs, indicating the absence of intersection of three 2 (2_1) axes.

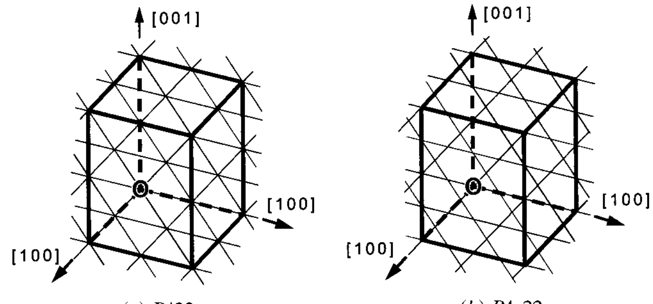

Figure 12
[211] projection arrangements of 2-fold-rotation and 2_1-screw axes of (*a*) *P*422 and (*b*) $P4_222$, which are observable by using three reflection pairs $(0\bar{1}1, 01\bar{1})$, $(10\bar{2}, \bar{1}02)$ and $(1\bar{1}\bar{1}, \bar{1}11)$.

space groups from one coherent CBED pattern taken at any probe position. We describe a retrieval procedure of the intersection characteristics of the 2 (2_1) axes from one coherent CBED pattern at a probe position where the 2 (2_1) axes do not intersect. The space-group pair of No. 15 (*I*422, $I4_122$) is taken as an example. Figs. 16(*a*) and 16(*b*) show the arrangements of the observable 2 (2_1) axes of *I*422 and $I4_122$ in the [111] projection, when three reflection pairs $(0\bar{1}1, 01\bar{1})$, $(10\bar{1}, \bar{1}01)$ and $(\bar{1}10, 1\bar{1}0)$ are used for observing the interference fringes. Figs. 17(*a*) and 17(*b*) show simulation patterns for *I*422 and $I4_122$ models under conditions where the probe is not positioned on a 2 (2_1) axis. Line pairs 1, 2, 3 and 4 are

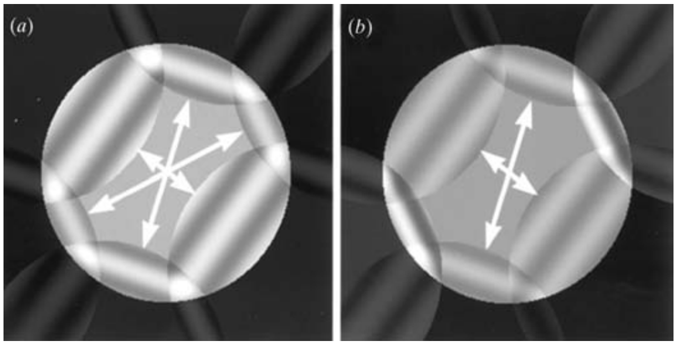

Figure 13
[211] coherent CBED patterns simulated for the $P422$ and $P4_222$ models for the electron probe positions O of Figs. 12(a) and 12(b). (a) exhibits three sets of mirror symmetry as indicated by the arrows, conforming to the intersection of three perpendicular 2 (2_1) axes at position O in Fig. 12(a), but (b) shows only two sets of mirror symmetry, indicating the absence of intersection of three 2 (2_1) axes.

Table 6
Incidences available for the distinctions of space-group sets.

No. 2	$P312$, ($P3_112$, $P3_212$)	[1$\bar{1}$01]
No. 3	$P321$, ($P3_121$, $P3_221$)	[11$\bar{2}$3]
No. 5	$P622$, ($P6_222$, $P6_422$)	[11$\bar{2}$3]
No. 7	$P6_322$, ($P6_122$, $P6_522$)	[11$\bar{2}$3]
No. 12	$P422$, $P4_222$	[321], [211], [112]*
No. 13	$P42_12$, $P4_22_12$	[211]
No. 15	$I422$, $I4_122$	[111]
No. 18	$P432$, $P4_232$	[321], [211]*
No. 20	$I432$, $I4_132$	[111]
No. 21	$F432$, $F4_132$	[432]

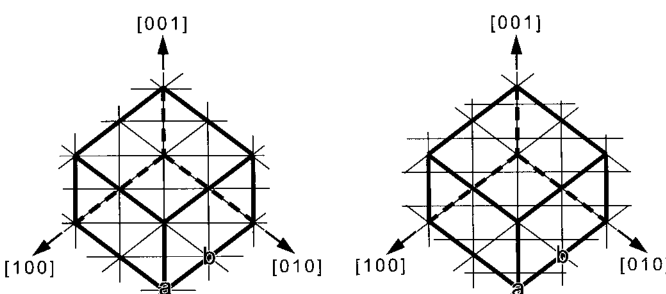

(a) $P422$ (b) $P4_222$

Figure 14
[112] projection arrangements of 2-fold-rotation and 2_1-screw axes of (a) $P422$ and (b) $P4_222$, which are observable by using four reflection pairs (1$\bar{1}$0, $\bar{1}$10), (11$\bar{1}$, $\bar{1}\bar{1}$1), ($\bar{2}$01, 20$\bar{1}$) and (0$\bar{2}$1, 02$\bar{1}$).

drawn on the peaks of the fringe pairs with a distance of $|\mathbf{g}|$. Lines 1c, 2c, 3c and 4c are drawn at the midpoints of the line pairs 1, 2, 3 and 4, respectively. Lines 5c–7c and 8c–11c are drawn by the same procedure for the different fringe pairs 5–7 and 8–11, respectively. It is seen that there exist points where the midway lines in the three different orientations intersect. Since the midway lines move as an entire set with the shift of the probe position, the relative positions between the lines in different orientations do not change. The intersection characteristics of the 2 (2_1) axes are always seen somewhere in the pattern irrespective of the probe position. In other words, the lines of Fig. 17(a) express the relative arrangement of the 2 (2_1) axes of $I422$ in the [111] projection (Fig. 16a). Fig. 17(b) shows the arrangements of the midway lines of a simulated coherent CBED patterns of a model of $I4_122$ for a point where the 2 (2_1) axes do not intersect. It is seen that no three midway lines intersect at a point, indicating the space group to be not $I422$ but $I4_122$. Thus, space group $I422$ can be distinguished from $I4_122$ by using any single coherent CBED pattern. The other space-group sets can also be distinguished from a single coherent CBED pattern by the same procedure.

The analysis described in the present paper allows us to distinguish the ten space-group sets that have principal rotation and screw axes and secondary 2 (2_1) axes. By adding the two space-group sets investigated by Tsuda *et al.*, the 12 space groups (Nos. 2, 3, 5, 7, 12, 13, 15–18, 20, 21) in the 23 indistinguishable space-group sets are distinguished by the coherent CBED method. The analysis does not directly distinguish whether the principal axes are rotation axes or screw ones but does distinguish the arrangements of the secondary 2 (2_1) axes. Thus, the present method cannot distinguish the eight space-group sets of Nos. 1, 4, 6, 8, 9, 10, 11 and 14, which do not have 2 (2_1) axes perpendicular to the principal axes. The remaining three space groups of Nos. 19, 22 and 23 are enantiomorphic space-group pairs, which have 2 (2_1) axes perpendicular to the principal axes.

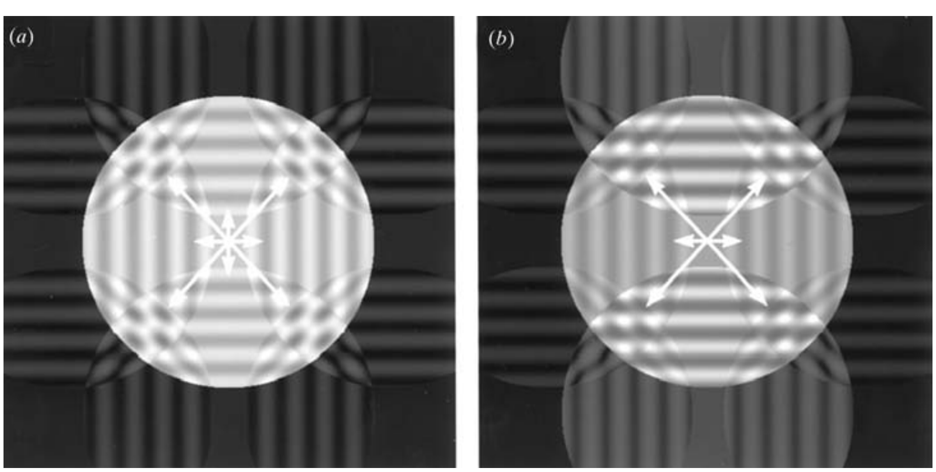

Figure 15
[112] coherent CBED patterns simulated for the $P422$ and $P4_222$ models for the electron probe positions a of Figs. 14(a) and 14(b). (a) exhibits four sets of mirror symmetry, conforming to the intersection of four perpendicular 2 (2_1) axes at position a in Fig. 14(a), but (b) shows only three sets of mirror symmetry, indicating the absence of intersection of four 2 (2_1) axes.

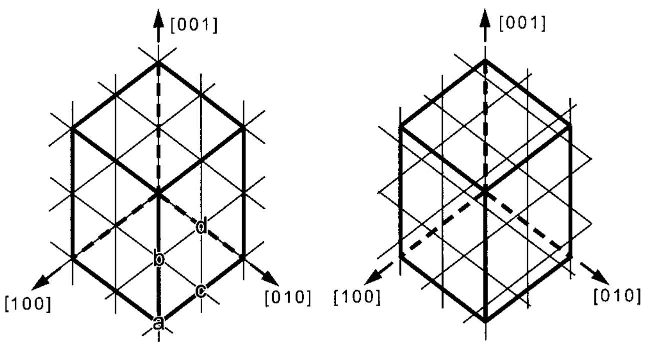

(*a*) *I*422 (*b*) *I*4$_1$22

Figure 16
[111] projection arrangements of 2-fold-rotation and 2_1-screw axes of (*a*) *I*422 and (*b*) *I*4$_1$22, which are observable by using three reflection pairs $(0\bar{1}1, 01\bar{1})$, $(10\bar{1}, \bar{1}01)$ and $(\bar{1}10, 1\bar{1}0)$.

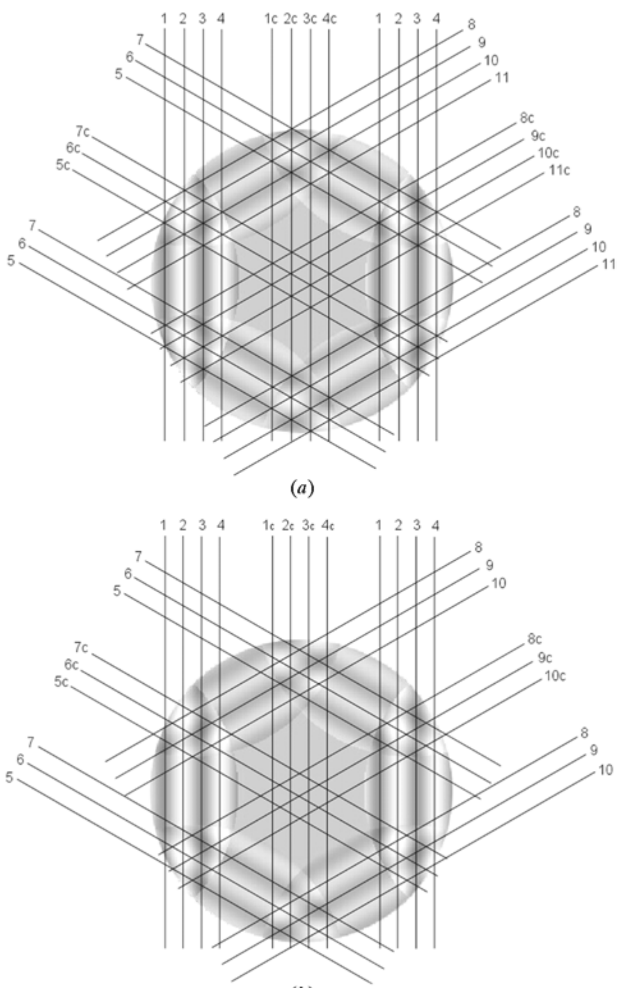

Figure 17
Retrieval procedure of the intersection characteristics of the 2 (2_1) axes from one coherent CBED pattern under conditions where the probe is not positioned on a 2 (2_1) axis. The midway lines 1*c*–11*c* of the line pairs 1–11 show the arrangements of the 2 (2_1) axes of (*a*) *I*422 and (*b*) *I*4$_1$22 in the [111] projection.

5. Conclusions

It has been found that Tsuda *et al.*'s analysis can be extensively applied to distinguish between the principal rotation and screw axes of the space groups that have 2-fold-rotation axes perpendicular to the principal axes. The method has allowed us to identify the ten space-group sets that have been indistinguishable so far. We are planning to confirm the present result experimentally by taking the coherent CBED patterns of real crystals. In a forthcoming paper, we will report a coherent CBED method to distinguish enantiomorphic space-group pairs.

References

Buxton, B. F., Eades, J. A., Steeds, J. W. & Rackham, G. M. (1976). *Philos. Trans. R. Soc. London*, **281**, 171–194.
Cowley, J. M. (1979). *Ultramicroscopy*, **4**, 435–450.
Dowell, W. C. T. & Goodman, P. (1973). *Philos. Mag.* **28**, 471–473.
Gjønnes, J. & Moodie, A. F. (1965). *Acta Cryst.* **19**, 65–67.
Goodman, P. (1975). *Acta Cryst.* A**31**, 804–810.
Goodman, P. & Johnson, A. W. S. (1977). *Acta Cryst.* A**33**, 997–1001.
Goodman, P. & Secomb, T. W. (1977). *Acta Cryst.* A**33**, 126–133.
International Tables for X-ray Crystallography (1952). Vol. I, edited by N. F. M. Henry & K. Lonsdale. Birmingham: Kynoch Press.
McCallum, B. C. & Rodenburg, J. M. (1993). *Ultramicroscopy*, **52**, 85–99.
Ou, H. J. & Cowley, J. M. (1988). Proc. 46th Annual Meeting of the Electron Microscopy Society of America, p. 882.
Spence, J. C. H. (1978). Proc. 9th International Congress on Electron Microscopy, Toronto, Canada, p. 554.
Steeds, J. W., Midgley, P. A., Spellward, P. & Vincent, R. (1995). *Electron Holography*, edited by A. Tonomura, L. F. Allard, G. Pozzi, D. C. Joy & Y. A. Ono, pp. 277–286. Amsterdam: Elsevier Science BV.
Tanaka, M. (1989). *J. Electron Microsc. Tech.* **13**, 27–39.
Tanaka, M., Saito, R. & Sekii, H. (1983). *Acta Cryst.* A**39**, 357–368.
Tanaka, M., Sekii, H. & Nagasawa, T. (1983). *Acta Cryst.* A**39**, 825–837.
Tanaka, M., Takayoshi, H., Ishida, M. & Endo, Y. (1985). *J. Phys. Soc. Jpn*, **54**, 2870–2974.
Tanaka, M. & Terauchi, M. (1985). *Convergent-Beam Electron Diffraction.* Tokyo: JEOL-Maruzen.
Tanaka, M., Terauchi, M. & Kaneyama, T. (1988). *Convergent-Beam Electron Diffraction II.* Tokyo: JEOL-Maruzen.
Tanaka, M., Terauchi, M. & Tsuda, K. (1994). *Convergent-Beam Electron Diffraction III.* Tokyo: JEOL-Maruzen.
Terauchi, M., Tsuda, K., Kamimura, O., Tanaka, M., Kaneyama, T. & Honda, T. (1994). *Ultramicroscopy*, **54**, 268–275.
Tinnappel, A. (1975). PhD thesis, Technical University, Berlin, Germany.
Tsuda, K., Saitoh, K., Terauchi, M., Tanaka, M. & Goodman, P. (2000). *Acta Cryst.* A**56**, 359–369.
Tsuda, K. & Tanaka, M. (1996). *J. Electron Microsc.* **45**, 59–63.
Tsuda, K., Terauchi, M., Tanaka, M., Kaneyama, T. & Honda, T. (1994). *J. Electron Microsc.* **43**, 173–175.
Vine, W. J., Vincent, R., Spellward, P. & Steeds, J. W. (1992). *Ultramicroscopy*, **41**, 423–428.
Zuo, J. M. & Spence, J. C. H. (1993). *Philos. Mag.* **68**, 1055–1078.